Available online at www.sciencedirect.com
SCIENCE DIRECT®
Physica B 358 (2005) 138–152
PHYSICA B
www.elsevier.com/locate/physb

Comparative Raman studies of Sr_2RuO_4, $Sr_3Ru_2O_7$ and $Sr_4Ru_3O_{10}$

M.N. Iliev[a,*], V.N. Popov[b], A.P. Litvinchuk[a], M.V. Abrashev[b], J. Bäckström[c,1], Y.Y. Sun[a], R.L. Meng[a], C.W. Chu[a,d]

[a]*Department of Physics and Texas Center for Superconductivity and Advanced Materials, University of Houston, Houston, Texas 77204-5002, USA*
[b]*Faculty of Physics, University of Sofia, 1164 Sofia, Bulgaria*
[c]*Department of Applied Physics, Chalmers University of Technology, S-41296 Göteborg, Sweden*
[d]*Hong Kong University of Science and Technology, Hong Kong, China*

Received 3 December 2004; received in revised form 31 December 2004; accepted 31 December 2004

Abstract

The polarized Raman spectra of layered ruthenates of the $Sr_{n+1}Ru_nO_{3n+1}$ ($n = 1, 2, 3$) Ruddlesden–Popper series were measured between 10 and 300 K. The phonon spectra of $Sr_3Ru_2O_7$ and $Sr_4Ru_3O_{10}$ confirmed earlier reports for correlated rotations of neighboring RuO_6 octahedra within double or triple perovskite blocks. The observed Raman lines of A_g or B_{1g} symmetry were assigned to particular atomic vibrations by considering the Raman modes in simplified structures with only one double or triple RuO_6 layer per unit cell and by comparison to the predictions of lattice dynamical calculations for the real Pban and Pbam structures. Along with discrete phonon lines, a continuum scattering, presumably of electronic origin, is present in the zz, xx and xy, but not in the $x'y'$ and zx spectra. Its interference with phonons results in Fano shape for some of the lines in the xx and xy spectra. The temperature dependences of phonon parameters of $Sr_3Ru_2O_7$ exhibit no anomaly between 10 and 300 K where no magnetic transition occur. In contrast, two B_{1g} lines in the spectra of $Sr_4Ru_3O_{10}$, corresponding to oxygen vibrations modulating the Ru–O–Ru bond angle, show noticeable hardening with ferromagnetic ordering at 105 K, thus indicating strong spin-phonon interaction.

PACS: 78.30.Hv; 63.20.Dj; 75.30.DS; 75.50.Ee

Keywords: Raman spectra; Layered ruthenates; Magnetic ordering effects

*Corresponding author. Tel.: +7137438209; fax: +7137438201.
E-mail address: miliev@uh.edu (M.N. Iliev).
[1]*Present address*: Permascand AB, Box 42, SE-84010 Ljungawerk, Sweden.

0921-4526/$ - see front matter © 2005 Elsevier B.V. All rights reserved.
doi:10.1016/j.physb.2004.12.069

1. Introduction

The properties of layered ruthenates $Sr_{n+1}Ru_nO_{3n+1}$ ($n = 1, 2, 3$), known as the Ruddlesden–Popper series, exhibit strong dependence on the number of RuO_6 octahedral layers. Sr_2RuO_4 ($n = 1$) is p-wave superconductor [1,2], $Sr_3Ru_2O_7$ ($n = 2$) is nearly ferromagnetic (enhanced paramagnetic) metal [3], whereas $Sr_4Ru_3O_{10}$ ($n = 3$, $T_C = 105\,K$) is a ferromagnetic metal [5,6]. There are indications that the variations with n of the magnetic and transport properties of $Sr_{n+1}Ru_nO_{3n+1}$ are partly related to the structural distortions in $Sr_3Ru_2O_7$ and $Sr_4Ru_3O_{10}$. While the structure of Sr_2RuO_4 is tetragonal ($I4/mmm$, No. 139, Fig. 1) and the Ru–O–Ru angle in the ab plane is 180°, the structures of $Sr_3Ru_2O_7$ (Pban, No. 50) and $Sr_4Ru_3O_{10}$ (Pbam, No. 55) are orthorhombic due to correlated rotations about the c-axis of the neighboring corner-sharing octahedra within each layer of the double or triple perovskite blocks [3–6]. These rotations result in decrease of the Ru–O–Ru angle in the ab plane to 166° for $Sr_3Ru_2O_7$ and 169° for the outer layers and 158° for the middle layers of $Sr_4Ru_3O_{10}$, respectively. The Sr-based ruthenates, however, are less distorted than corresponding Ca-based compounds. Indeed, besides being rotated around the c axis, the RuO_6 octahedra in Ca_2RuO_4 (Pbca, No. 61) [2] and $Ca_3Ru_2O_7$ ($A2_1ma$, No. 36) [7] are additionally tilted around an axis lying in the RuO_2 plane.

The coupling among the charge, lattice and spin degrees of freedom in $(Ca, Sr)_{n+1}$ Ru_nO_{3n+1} compounds has been subject of several magnetotransport [3,6], pressure [8,9] and Raman [9–12] studies. The polarization-, temperature-, pressure- and substitution-dependent Raman spectra allowed observation of the two-magnon scattering, opening of the spin gap, and pressure- and substitution-induced variations in metal–insulator transition in Ca_2RuO_4 [9], $Ca_{2-x}Sr_xRuO_4$ [12] and $Ca_3Ru_2O_7$ [10,9], as well as spin gap and strong direction-dependent–electron–phonon interaction in Sr_2RuO_4 [11]. The latter studies illustrated the ability of Raman scattering to provide information on the interplay of spin, charge, and lattice degrees

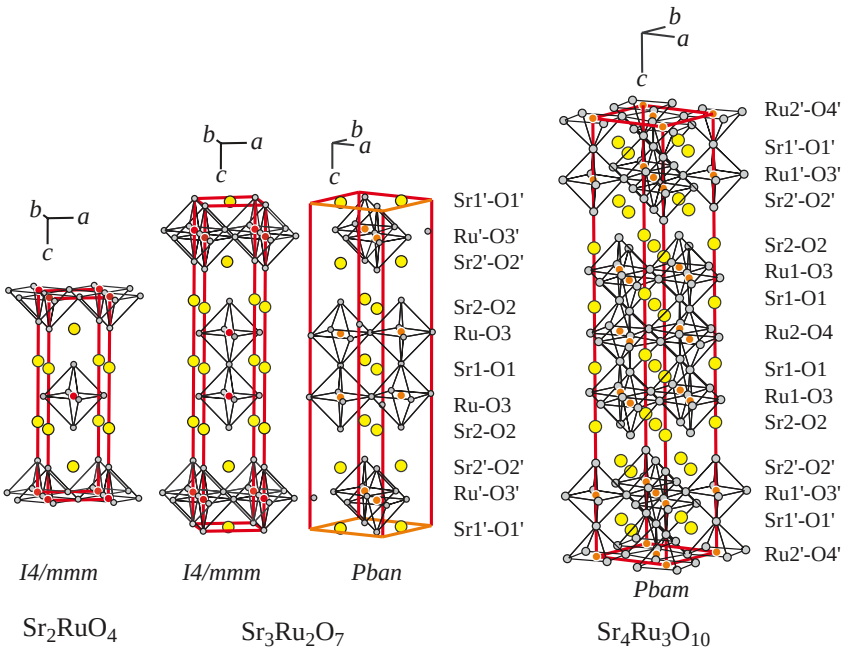

Fig. 1. Units cells of Sr_2RuO_4 ($I4/mmm$), $Sr_3Ru_2O_7$ ($I4/mmm$ and Pban) and $Sr_4Ru_3O_{10}$ (Pbam).

of freedom. To our knowledge, there are yet no reports on the Raman spectroscopy of double-layer $Sr_3Ru_2O_7$ and triple-layer $Sr_4Ru_3O_{10}$. The Raman spectra of these materials and their variation with temperature are of definite interest as they contain information about the local structure, electron–phonon, spin–phonon interactions and their dependence on the number of RuO_6 layers. An essential precondition for correct analysis and understanding of complex structure–properties relationships is the assignment of the Raman lines to particular atomic motions.

In this work we present results of comparative polarization- and temperature-dependent Raman studies of Sr_2RuO_4, $Sr_3Ru_2O_7$ and $Sr_4Ru_3O_{10}$ between 10 and 300 K. The spectra of $Sr_3Ru_2O_7$ and $Sr_4Ru_3O_{10}$ provide clear evidence for a structure containing correlated rotations of RuO_6 octahedra within perovskite blocks. On the basis of their symmetry, considering corresponding modes in simplified tetragonal structures, containing RuO_6 rotations, and by comparison to the predictions of lattice dynamical calculations (LDC) for the real orthorhombic Pban and Pbam structures, the observed Raman lines of $Sr_3Ru_2O_7$ and $Sr_4Ru_3O_{10}$ are assigned to definite phonon modes. Except for phonon lines, a continuum scattering, presumably of electronic origin, with components of A_g (xx and zz) and B_{1g} (xy) symmetry is present in the whole temperature range. Its interference with phonons results in Fano shape for some of the lines in the xx and xy spectra. Phonon anomalies related to magnetic ordering at $T_C = 105$ K are observed in the temperature-dependent spectra of $Sr_4Ru_3O_{10}$.

2. Samples and experimental

Rectangular platelet-like single crystals of $Sr_{n+1}Ru_nO_{3n+1}$ ($n = 1, 2, 3$) with typical size $1 \times 1 \times 0.2\,mm^3$ were grown using $SrCO_3$ and RuO_2 as starting materials and $SrCl_2$ as a flux. The compositions Sr_2RuO_4, $Sr_3Ru_2O_7$, and $Sr_4Ru_3O_{10}$ were obtained by varying the $SrCO_3$:$SrCl_2$ ratio and temperature profiles. The temperature profile was basically as follows: (1) temperature increases to 1400–1500 °C in 7 h and then constant temperature for 25 h, (2) cooling down to 1250–1350 °C at a rate of 2°/h, (3) further cooling to room temperature in 1 h.

The X-ray diffraction showed that the lattice parameters of all three compounds corresponded to the ones known from the literature. It was also established and further confirmed by Raman polarization selection rules that the large surfaces of the crystal platelets were parallel to the (0 0 1) plane and their edges were along either {1 0 0} or {1 1 0} directions.

Raman spectra were collected using Jobin–Yvon HR640 spectrometer equipped with microscope (100× or 50× objective, focus spot size 1–3 μm), notch filters and liquid–nitrogen-cooled charge-coupled device (CCD) detector. The He–Ne (632.8 nm) and Ar^+ (514.5 and 488.0 nm) laser lines were used for excitation. The lack of spurious signals from impurity phases was verified by the reproducibility of the spectra and their strict polarization. Given the crystallographic directions were known, measurements could be done in several exact backward scattering configurations: $z(xx)\bar{z}$, $z(yy)\bar{z}$, $z(xy)\bar{z}$, $z(x'x')\bar{z}$, $z(x'y')\bar{z}$, $y(zz)\bar{y}$, $y(zx)\bar{y}$, $y(xx)\bar{y}$, $y(x'x')\bar{y}$. The first and fourth letters in these notations stay for the directions of incident and scattered light, whereas their polarizations are denoted by the second and third letters, respectively. As $x \equiv [1\,0\,0]$ and $y \equiv [0\,1\,0]$ are indistinguishable, x and y are interchangeable. The same is valid for $x' \equiv [1\,1\,0]$ and $y' \equiv [1\,\bar{1}\,0]$. Further, the short notations xx, zz, $x'x'$, $x'y'$ and zx, referring to the light polarization, will also be used.

3. Raman active phonons in Sr_2RuO_4, $Sr_3Ru_2O_7$ and $Sr_4Ru_3O_{10}$

A phonon mode is Raman active if the atomic motions modulate the unit cell polarizability and hence the polarizability of the crystal as a whole. The motion of atoms at sites, which are centers of symmetry do not change the cell polarizability and the corresponding phonon modes are not Raman active. Therefore the total number of Raman modes is determined by both, the crystal symmetry

and the number of atoms at noncentrosymmetrical sites in the primitive cell.

The primitive cell of Sr_2RuO_4, which is twice smaller than the body-centered $I4/mmm$ unit cell shown in Fig. 1, contains one formula unit. Ru and planar oxygen atoms (O1) are at centers of symmetry and their vibrations are not Raman active. From symmetry considerations one expects four ($2A_{1g} + 2E_g$) Raman modes. The two A_{1g} modes correspond to stretching vibrations along z of Sr and apex oxygen (O2), whereas the two doubly degenerated E_g mode represent the vibrations of the same atoms in the xy plane.

The primitive cell of the idealized undistorted $Sr_3Ru_2O_7$ structure (without octahedral tilts) also contains one formula unit, whereas the unit cell of $I4/mmm$ symmetry is twice larger (Fig. 1). In this idealized structure the Sr1 and O1 atoms are at centers of symmetry and do not participate in Raman active modes. The remaining atoms participate in ten Γ-point ($4A_{1g} + B_{1g} + 5E_g$) Raman modes. Again, from symmetry considerations one can conclude that the four A_{1g} modes correspond to vibrations along z of Ru, Sr2, O2 and O3 (in phase), the B_{1g} mode represents the out-of-phase vibrations of O3, and the shapes of the E_g modes are determined by motions of these five types of atoms parallel to the xy plane.

The real orthorhombic Pban structure of $Sr_3Ru_2O_7$ can be obtained from the idealized $I4/mmm$ structure by ordered counter-phase rotations of RuO_6 octahedra around the z-axis. The x and y axes of the Pban structure are rotated by 45° with respect to those of the tetragonal one and the a and b-parameters are larger by factor $\sqrt{2}$. Compared to the idealized $I4/mmm$ structure, the number of Raman-allowed Γ-point phonons in the Pban structure increases from 10 to 72 ($12A_g + 16B_{1g} + 22B_{2g} + 22B_{3g}$) due to the larger primitive cell (it coincides with the unit cell, shown in Fig. 1 and contains four formula units), absence of the cell centering, lifting of E_g degeneracy, and appearance of new modes related to RuO_6 rotations. One should not expect, however, observation of such a large number of Raman lines, as to each A_{1g}, B_{1g} or E_g tetragonal mode one can juxtapose, respectively, a pair of two A_g, two B_{1g} or $B_{2g} + B_{3g}$ orthorhombic modes, which involve practically the same atomic vibrations and have very close frequencies. Experimentally, these pairs will be observed as a single line. While the shapes of the Raman modes originating from the Raman allowed tetragonal modes remain practically the same, the shapes of some of the new modes are not so obvious.

The idealized structure (without octahedral tilts) of triple-layer $Sr_4Ru_3O_{10}$, which is not shown, is also of $I4/mmm$ symmetry. Ru and O atoms of the internal Ru–O planes are at centers of symmetry and their vibrations are not Raman active. The rest atoms participate in 14 Γ-point ($6A_{1g} + B_{1g} + 7E_g$) Raman modes. The real structure, however, is orthorhombic and has been refined as Pbam (Fig. 1) [5]. Here again all atoms, except for Ru2 and Ru2′, are in non-centrosymmetrical sites and participate in Raman-active modes. From symmetry considerations in total 96 ($20A_g + 20B_{1g} + 28B_{2g} + 28B_{3g}$) Γ-point modes are Raman allowed. Like in the case of $Sr_3Ru_2O_7$, however, many of these modes are practically degenerated in pairs and lower number of Raman lines is expected. It is plausible to expect some similarities in the Raman spectra of $Sr_4Ru_3O_{10}$ and $Sr_3Ru_2O_7$ as the nearest surrounding for part of the atoms is practically the same in both compounds.

As it follows from above, given the crystal symmetry is known, one can predict the number and symmetry of the Raman lines expected in the spectra. Experimentally, the number of observed lines is lower as some lines are of very low intensity and others may be superimposed. The assignment of experimentally observed lines to definite atomic vibrations is not straightforward except for relatively simple structures with small number of modes of given symmetry. Such is the case of the two A_{1g} modes of Sr_2RuO_4 observed experimentally at 200 and 545 cm^{-1} (see the next section). As these modes correspond to stretching vibrations of Sr and O2, it is plausible to assign the low-frequency line to vibrations of heavier Sr and the high-frequency line to vibrations of lighter oxygen atoms. As a rule, however, the Raman modes in materials with more complicated structure are strongly mixed and of complex shape, which does

not allow simple approach for determination of their frequency.

For assignment of the experimentally observed Raman lines in the spectra of $Sr_3Ru_2O_7$ and $Sr_4Ru_3O_{10}$ we will apply a two-way approach. The first approach is based on the reasonable assumption that the interaction between double(triple) Ru–O slabs is weak and the only important distortions are the rotations of the RuO_6 octahedra. Therefore, instead of real Pban and Pbam structures, we may consider simplified structures with unit cell containing only one double(triple) layer. We will argue that the experimentally observed lines of A_{1g} and B_{1g} symmetry correspond to the modes expected for the simplified structures and will make a tentative assignment. The frequency of the modes of similar shape in Sr_2RuO4, $Sr_3Ru_2O_7$ and $Sr_4Ru_3O_{10}$ is expected to vary mainly due to changes of the bond lengths. Therefore, further verification of Raman line assignment (e.g., to apex oxygen vibrations) may be obtained by comparison of experimentally observed differences of Raman frequencies with those expected from the differences in the corresponding bond lengths.

Within a second approach, we will compare the experimentally observed frequencies with those predicted by lattice dynamical calculations (LDC) for the exact structures of $Sr_3Ru_2O_7$ and $Sr_4Ru_3O_{10}$. The calculations were done using a shell model described in detail in Ref. [13]. This model gives an adequate description of the vibrations in perovskitelike structures because it accounts for their predominant ionicity. The ionic interactions are represented by long-range Coulomb potentials and short-range repulsive potentials of the Born–Mayer form ae^{-br} where a and b are constants and r is the interionic separation. The deformation of the electron charge density of the ions is described in the dipole approximation considering each atom as consisting of a point charged core and a concentric spherical massless shell with charge Y. Each core and its shell are coupled together with a force constant k giving rise to the free ionic polarizability $\alpha = Y^2/k$. The model parameters for the strontium, ruthenium, and oxygen ions and their interaction potentials were taken from a previous study of simpler compounds with perovskitelike structure [13,14].

4. Results and discussion

4.1. Sr_2RuO_4

The polarized Raman spectra of Sr_2RuO_4 at room temperature as obtained with 488.0 nm excitation are shown in Fig. 2. Three of the four $(2A_{1g} + 2E_g)$ Raman allowed phonons are observed at 200 cm^{-1} (A_{1g}, Sr vibrations along z), 247 cm^{-1} (E_g, apex oxygen vibrations in the xy plane), and 545 cm^{-1} (A_{1g}, apex oxygen vibrations along z), in consistence with earlier reports of Udagawa et al. [15] and Sakita et al. [11]. The Raman phonon intensities I_ω exhibit clear resonant behavior. For example in the zz-polarized spectra the I_{545}/I_{200} ratio is 19.3 for 632.8 nm (1.96 eV), 4.2 for 514.5 nm (2.41 eV), and 3.5 for

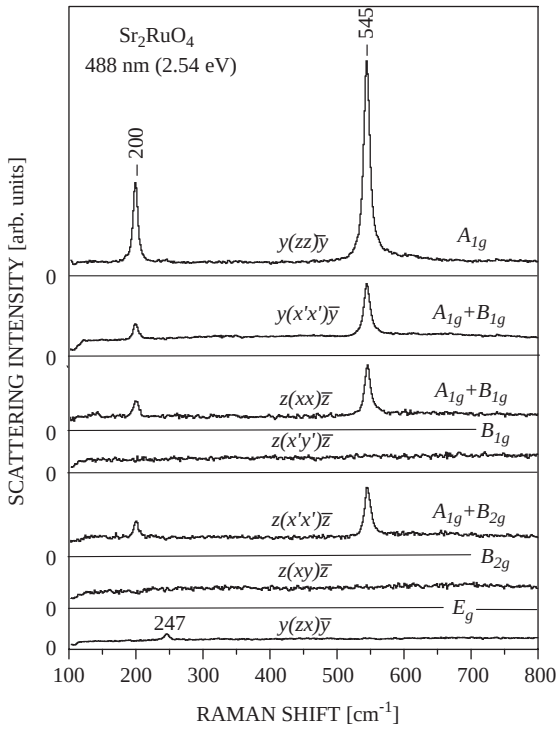

Fig. 2. Polarized Raman spectra of Sr_2RuO_4, obtained at room temperature with 488 nm excitation. A continuum background is present in all spectra.

488.0 nm (2.54 eV) excitations, respectively. In the xx polarized spectra the corresponding values are 2.1, 1.5, and 4.2. For all three excitation energies used, the $y(xx)\bar{y}$ and $z(xx)\bar{z}$ spectra were practically identical.

Except for the phonon lines, an electronic background was present in all spectra. The electronic Raman scattering for incident polarization parallel to the ab plane has previously been reported by Yamanaka et al. [16], who observed structureless continuum with A_{1g}, B_{1g} and B_{2g} components of comparable intensity. Our measurements have shown, however, that the $A_{1g}(xx)$ component of the continuum is much weaker than those of $B_{1g}(x'y')$ and $B_{2g}(xy)$ symmetry.

4.2. $Sr_3Ru_2O_7$

Polarized Raman spectra of $Sr_3Ru_2O_7$ measured at room temperature with 633, 515 and 488 nm laser line excitation are shown in Fig. 3. Five lines of A_g symmetry are clearly pronounced in the xx and zz spectra at 118, 165, 212, 395, and 577 cm^{-1}. Another two lines of B_{1g} symmetry are seen in the xy spectra at 306 and 377 cm^{-1}, but no lines of detectable intensity are observed in the $zx(zy)$ spectra where are allowed the modes of $B_{2g}(B_{3g})$ symmetry. The intensity of the Raman lines changes with excitation energy due to alteration of the resonance conditions. The relative intensities of the A_g line at 395 cm^{-1} and the two B_{1g} lines, however, remain nearly the same. This suggests that the three modes involve motions of same type of atoms, different from those with main contribution to the A_g mode at 577 cm^{-1}. The number of Raman lines in the spectra of $Sr_3Ru_2O_7$ is noticeably lower than in the corresponding spectra of $Ca_3Ru_2O_7$ [10]. This had to be

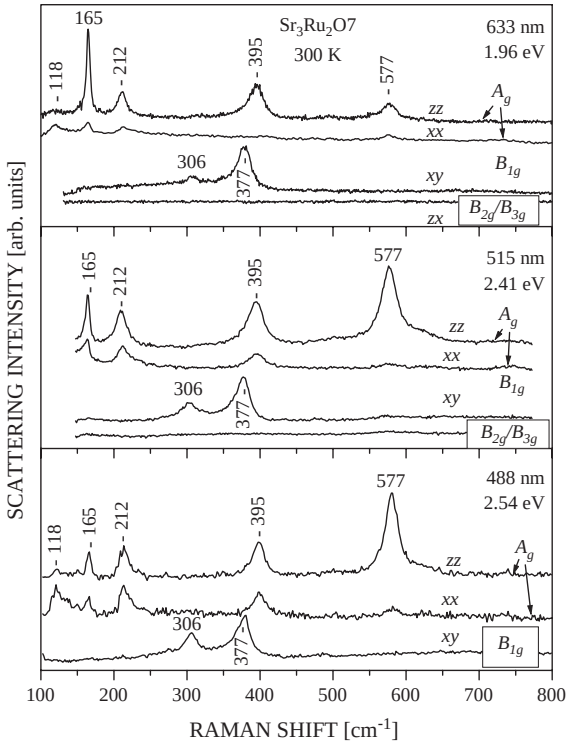

Fig. 3. Polarized Raman spectra of $Sr_3Ru_2O_7$, obtained at room temperature with 633, 515, and 488 nm excitation. Some curves are shifted vertically for clarity.

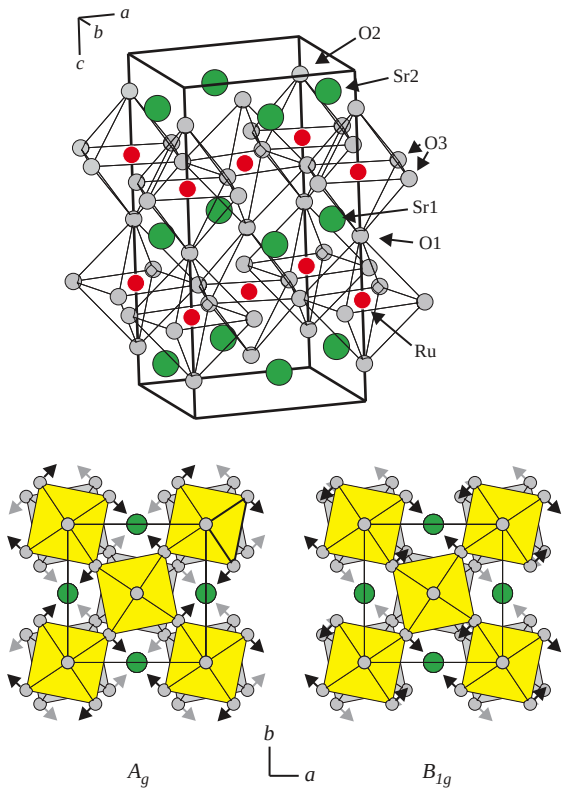

Fig. 4. Simplified distorted structure ($P4/nbm$) of $Sr_3Ru_2O_7$ with unit cell containing one double Ru–O layer. The distortion-activated A_g and B_{1g} modes are also shown.

expected as the structure of $Ca_3Ru_2O_7$ is more strongly distorted and the number of fully symmetrical modes allowed in *xx*, *yy* and *zz* configurations is higher.

As discussed in the previous section, instead of the real Pban structure, one can consider a simplified structure with unit cell containing only one double layer (Fig. 4). This structure is tetragonal ($P4/nbm$, No. 125, $Z = 2$) with the same *a* and *b* parameters as the real one, but twice shorter *c* parameter. The normal mode analysis gives $5A_{1g} + B_{1g} + 4B_{2g} + 11E_g$ Raman modes. Therefore one expects in the *xx* and *zz* spectra five Raman lines of A_g symmetry (A_{1g} in tetragonal notations), which is exactly the case. In the *xy* spectra one expects observation of four B_{1g} modes (B_{2g} in tetragonal notations), two of them involving mainly oxygen vibrations.

The Raman mode frequencies in ionic materials, such as transition metal oxides, are determined by the mass, charge, and bond lengths of participating atoms as well by the type of atomic motions (stretching, bending or rotational). Based on comparison to other perovskitelike oxides, the modes involving mainly vibration of heavier Ru and Sr or rotational vibrations of oxygens are expected in the frequency range below $250\,cm^{-1}$, the bending oxygen modes—between 200 and

Table 1
Calculated (for the Pban and $I4/mmm$ structures) and experimentally observed A_g/A_{1g} and B_{1g} phonon frequencies in $Sr_3Ru_2O_7$

Mode Pban	LDC Pban	Exp 300/10 K	Atomic motions	Mode $I4/mmm$	LDC	Mode $P4/nbm$
$A_g(1)$	117	118/138	RuO_6 rot			A_{1g}
$A_g(2)$	179	165/170	Ru(*z*), Sr2(*z*)	A_{1g}	180	A_{1g}
$A_g(3)$	210	213/225	Sr2(*z*), Ru(*z*)	A_{1g}	214	A_{1g}
$A_g(4)$	223	213/225				
$A_g(5)$	250					
$A_g(6)$	254					
$A_g(7)$	402	395/409	O3(*z*)	A_{1g}	512	A_{1g}
$A_g(8)$	402	395/409				
$A_g(9)$	520					
$A_g(10)$	522					
$A_g(11)$	580	577/581	O2(*z*)	A_{1g}	589	A_{1g}
$A_g(12)$	580	577/581				
$B_{1g}(1)$	108					
$B_{1g}(2)$	109					
$B_{1g}(3)$	162					B_{2g}
$B_{1g}(4)$	162					
$B_{1g}(5)$	181					B_{2g}
$B_{1g}(6)$	181					
$B_{1g}(7)$	337	306/316	O3(*z*, −*z*)	B_{1g}	310	B_{2g}
$B_{1g}(8)$	337	306/316				
$B_{1g}(9)$	378	377/380	O3(*xy*)			B_{2g}
$B_{1g}(10)$	378	377/380				
$B_{1g}(11)$	466					
$B_{1g}(12)$	466					
$B_{1g}(13)$	521					
$B_{1g}(14)$	521					
$B_{1g}(15)$	726					
$B_{1g}(16)$	726					

500 cm^{-1} and stretching oxygen modes—above 500 cm^{-1}. Our LDC for the Pban structure (Table 1) predicts that the A_g modes below 250 cm^{-1} are strongly mixed, each involving vibrations along z of Ru and Sr2 as well as RuO_6 rotations around z. In the $I4/mmm$ structure, however, the rotational motions (see Fig. 4), are not Raman active. Therefore, the 165 and 213 cm^{-1} lines, which are close to LDC frequencies predicted for both Pban and $I4/mmm$ structures, can tentatively be assigned to mixed vibrations of Ru and Sr along z. The line at 118 cm^{-1} is close to the LDC(Pban) frequency of 117 cm^{-1}, which has no partner in the LDC($I4/mmm$) data, is assigned to mainly RuO_6 rotations. The "soft"-mode temperature behavior of the latter line is also typical for a rotational mode. As to the two high-frequency A_g modes, with great certainty, confirmed by LDC, they correspond to out-of-plane in-phase vibrations of O3 (395 cm^{-1}) and stretching vibrations of O2 (577 cm^{-1}). The latter frequency is higher than that of the corresponding apex oxygen vibrations in Sr_2RuO_4 (545 cm^{-1}), which can be explained considering the bond-length changes. Indeed, it is plausible to assume that the force constants k_{O-M} between O and the ion M follows the simple $Z_O Z_M / r^3_{O-M}$ relation, where Z_O and Z_M are the charges of the oxygen and cation, respectively, and r_{O-M} is the oxygen–cation bond length. This relation is valid for harmonic ionic crystals and shown to apply for perovskitelike transition metal oxides [17,18]. Taking into account that $\omega^2 = k/m$ and restricting interactions to only nearest-neighbors (Ru and Sr), one obtains for the particular case of O2 stretching vibrations

$$\omega^2 \propto Z_{Ru}/r^3_{O-Ru} + Z_{Sr}/r^3_{O-Sr}, \quad (1)$$

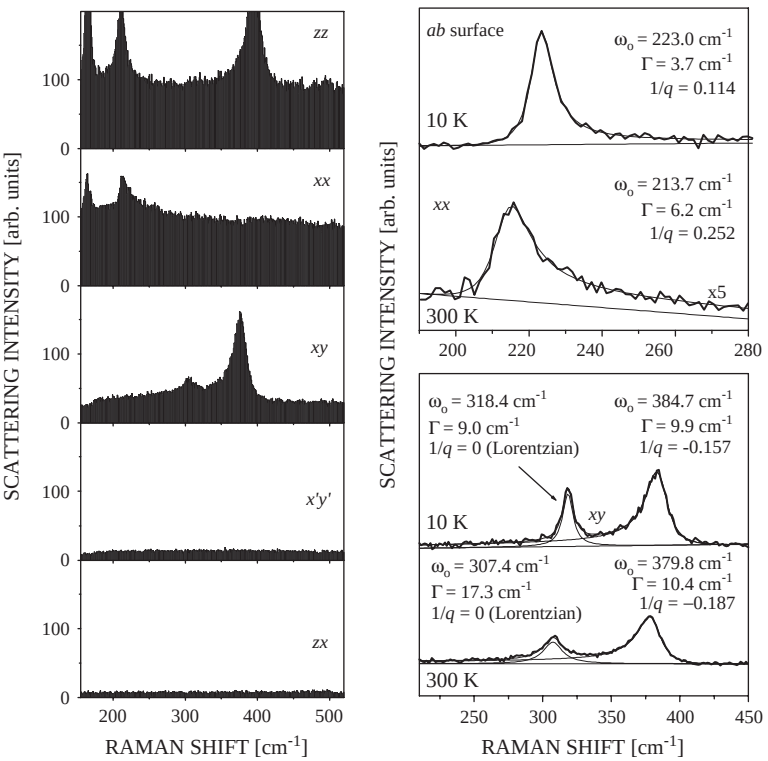

Fig. 5. Left panel: continuum scattering from $Sr_3Ru_2O_7$ as obtained with 633 nm excitation for several exact scattering configurations. Right panels: Fano fit of the 213/223 cm^{-1} A_g (xx) and 377/384 cm^{-1} B_{1g} lines. The fit parameters are also given.

where $Z_{Ru} = 4$, $Z_{Sr} = 2$, and the values of r_{O-Ru} and r_{O-Sr} are respectively 2.016 and 2.459 Å for $Sr_3Ru_2O_7$ [4] and 2.059 and 2.440 Å for Sr_2RuO_4 [19]. Using these values one obtains $\omega_{Sr_3Ru_2O_7}/\omega_{Sr_2RuO_4} = 1.045$, which is close to the experimental ratio of 1.059.

There is little doubt too, that the two experimentally observed lines in the *xy* spectra correspond to the two oxygen B_{2g} modes of the distorted $P4/nbm$ structure. The main atomic motions are out-of-phase vibrations along *z* of O3 (306 cm^{-1}) and "scissors-like" bendings of O3 parallel to the *xy* plane (377 cm^{-1}). The shape of the latter mode is also shown in Fig. 4.

Along with the phonon lines, a structureless background of A_g(*zz* and *xx*), and B_{1g} (*xy*) symmetry, but not of B_{2g}/B_{3g} (*zx* or *zy*) symmetry, is also present in the spectra. This is illustrated in Fig. 5 for room temperature spectra taken with 633 nm excitation. The observation of relatively strong *zz*-polarized continuum was somewhat unexpected as the ARPES measurements [20] and band structure calculations [21] provide evidence for quasi-two-dimensional Fermi-surface sheets, in consistence with reports for large anisotropy of the electrical resistivity ($\rho_z/\rho_{xy} \approx 40$ at 300 K) [3]. The continuum-phonons interference is clearly pronounced only for incident radiation parallel to the *xy* plane through Fano shape of the 213 cm^{-1} A_g line in the *xx* spectra and the 377 cm^{-1} B_{1g} line in the *xy* spectra (Fig. 5). For a phonon coupled to electronic background, the Fano profile $I(\omega) = I_0(\varepsilon + q)^2/(1 + \varepsilon^2)$ is generally used to describe the line shape, where $\varepsilon = (\omega - \omega_0)/\Gamma$, ω_0 is the "bare" phonon frequency, Γ is the linewidth, and *q* is the asymmetry parameter. Both, $\Gamma = \pi\rho V^2$ and $q = t_p/(\pi\rho V t_e)$ depend on the electron–phonon interaction *V*, which can be written as $V = (t_e/t_p)\Gamma q$. t_e, t_p, and ρ are the electron and phonon transition probabilities, and the density of states of electronic excitations, respectively. Under the assumption of negligible temperature dependence of $t_e$and t_p, the temperature dependence of *V* will be reflected by Γq. Using the values of Γ, and *q* as obtained from the Fano fit of the experimental line profiles (see the data listed in Fig. 5), a conclusion can be made that *V* increases with decreasing temperature.

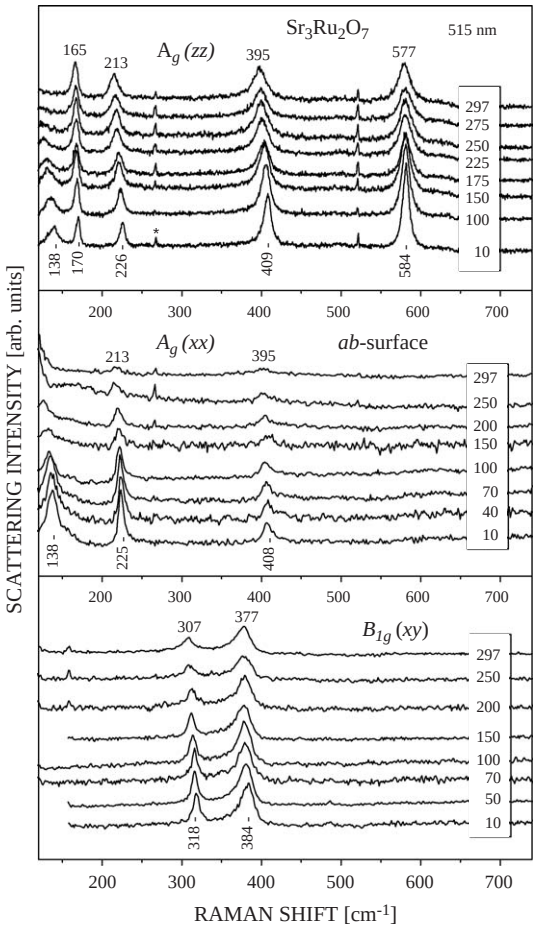

Fig. 6. Temperature-dependent polarized Raman spectra of $Sr_3Ru_2O_7$ between 10 and 300 K obtained with 515 nm excitation.

Fig. 6 shows the temperature-dependent *zz*, *xx* and *xy* Raman spectra of $Sr_3Ru_2O_7$ between 10 and 300 K. The variations of phonon frequencies and line widths with temperature exhibit no anomalies. The relative changes of frequency for all observable modes are summarized in Fig. 7. The low frequency A_g mode shows "soft"-mode behavior, its frequency decreasing by $\approx 15\%$ between 10 and 300 K, while the frequency of the highest mode remains practically unchanged. The continuum scattering in the *zz*, *xx* and *xy* spectra only slightly decreases with lowering temperature,

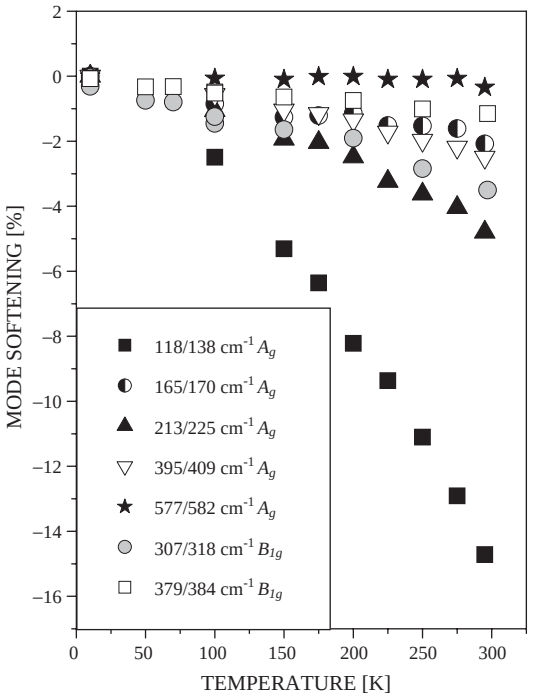

Fig. 7. Variations with T of the relative changes $[\omega(T)-\omega(10)]/\omega(10)$ of the A_g mode frequencies in $Sr_3Ru_2O_7$.

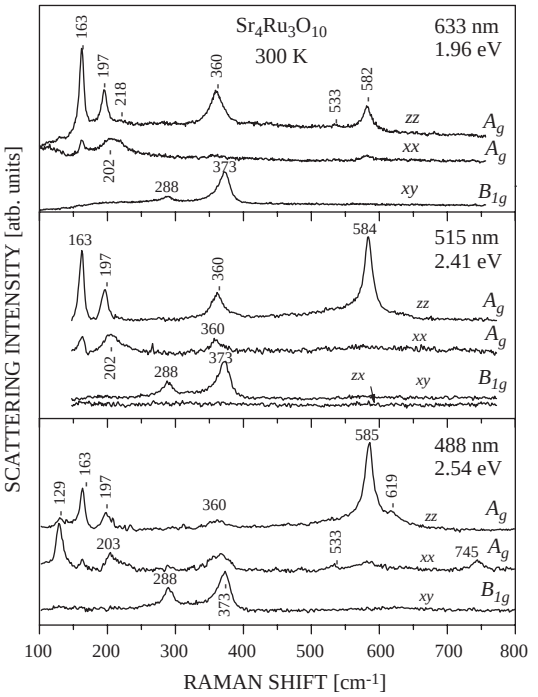

Fig. 8. Polarized Raman spectra of $Sr_4Ru_3O_{10}$, obtained at room temperature with 633, 515 and 488 nm excitation. Some curves are shifted vertically for clarity.

in contrast to the case of $Ca_3Ru_2O_7$, where a rapid suppression of the electronic background of B_{1g} symmetry has been observed below the metal-insulator transition at $T_{MI} \approx 48$ K [10]. The interaction between the continuum and phonons also decreases with lowering temperature, as evidenced from Fig. 5, where the $1/q$ values are compared at 10 and 300 K.

4.3. $Sr_4Ru_3O_{10}$

Fig. 8 shows the zz, xx, xy and zx spectra obtained at room temperature with 633, 515, and 488 nm excitation. The temperature variations of the spectra between 10 and 300 K are given in Fig. 9. Except for line shifts and appearance of additional weak lines, the spectral profiles and their dependence on scattering configuration and excitation wavelength resembles that of $Sr_3Ru_2O_7$. Lines of A_g symmetry are observed at room temperature at 129, 163, 195–203, 360–365, 533, 582–585, 619 and 745 cm^{-1}. The broad structure near 200 cm^{-1} in the xx spectra appears to be a superposition of two lines. This becomes evident at low temperatures where these two line are well separated. Like in the case of $Sr_3Ru_2O_7$, only two lines of B_{1g} symmetry are pronounced and the intensity of the B_{2g} and B_{3g} lines is below the detection limit.

To assign the Raman lines to particular phonon modes let us again consider the Raman modes in a simplified distorted tetragonal structure and compare the experimental frequencies to the prediction of lattice dynamical calculations for the real Pbam structure of $Sr_4Ru_3O_{10}$. The simplified structure $P4/mbm$ (No. 127, $Z = 2$), shown in Fig. 10, has only one triple layer in the unit cell. It is characterized by the same equal a and b parameters as the real structure, but twice shorter c parameter. From symmetry considerations $8A_{1g} +$

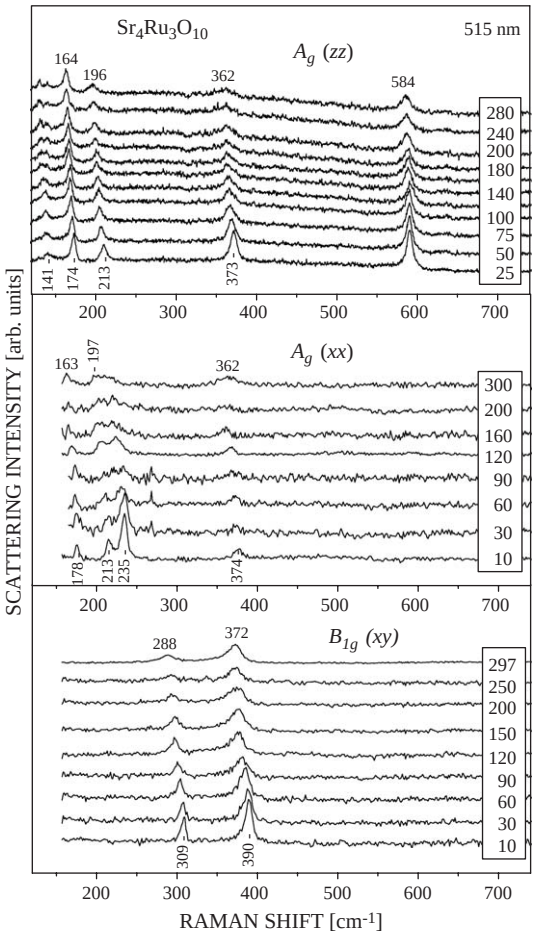

Fig. 9. Variation with T of the *zz*, *xx* and *xy* spectra of $Sr_4Ru_3O_{10}$.

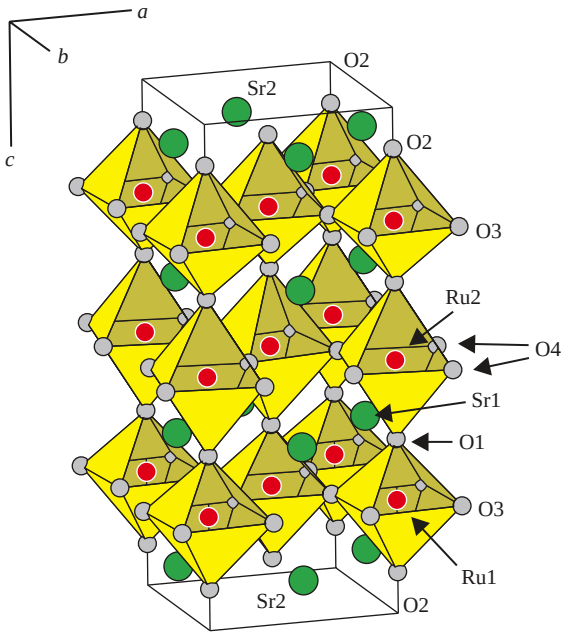

Fig. 10. Simplified distorted structure of $Sr_4Ru_3O_{10}$: $P4/mbm$, No. 127, $Z = 2$.

$2B_{1g} + 5B_{2g} + 14E_g$ modes are Raman active. The A_{1g} modes, allowed in *xx* and *zz* spectra, correspond to A_g modes in orthorhombic Pbam, whereas the tetragonal B_{2g} modes, allowed in the *xy* spectra, correspond to the orthorhombic B_{1g} modes. Compared to the simplified structure of $Sr_3Ru_2O_7$, there are three new $A_{1g}(A_g)$ modes corresponding to: (i) rotations of middle RuO_6 octahedra, (ii) vibrations along *z* of internal apex oxygen atoms (O1), (iii) vibrations along *z* of internal Sr1 atoms. The LDC predicts close frequencies for the rotational and Sr1 modes and our assignment of the new *xx* polarized A_g line, seen at low temperature at 235 cm^{-1} and also having a "soft"-mode temperature behavior, to rotational vibrations of middle RuO_6 octahedra is only tentative. The new A_g line at 745 cm^{-1}, seen in the *xx* spectra with 488 nm excitation, can tentatively be assigned to the vibrations along *z* of the inner O1 atoms. Using Eq. (1) with the experimental values of $r_{O1-Ru2} = 1.991$ Å, $r_{O1-Ru1} = 2.014$ Å and $r_{O2-Ru1} = 2.077$ Å, $r_{O2-Sr2'} = 2.380$ Å one obtains frequency of O1 vibrations along *z* should be by factor 1.35 higher than that of the outer apex oxygens (O2). This is in good agreement with the experimentally observed ratio of 745: 584 = 1.28. A comparison of phonon frequencies predicted by LDC with experimental data is given in Table 2.

The left panel of Fig. 11 illustrates the presence in the *zz*, *xx* and *xy* spectra of $Sr_4Ru_3O_{10}$ of scattering continuum. Like in the case of $Sr_3Ru_2O_7$, some lines exhibit clear Fano shape

Table 2
Calculated and experimentally observed A_{1g} and B_{1g} phonon frequencies in $Sr_4Ru_3O_{10}$. The corresponding modes in the simplified $P4/mbm$ structure are also given

Mode Pbam	LDC Pbam	Exp 300/10 K	Atomic motions	Mode $P4/mbm$	Mode Pbam	LDC Pbam	Exp 300/10 K	Atomic motions	Mode $P4/mbm$
$A_g^{(1)}$	90	129/140	outer RuO_6 rot in xy	A_{1g}	$B_{1g}^{(1)}$	147			
$A_g^{(2)}$	150	163/178	Ru1(z)Sr2(z)	A_{1g}	$B_{1g}^{(2)}$	151			
$A_g^{(3)}$	173				$B_{1g}^{(3)}$	175			B_{2g}
$A_g^{(4)}$	190	198/214	Sr2(z)Ru1(z)	A_{1g}	$B_{1g}^{(4)}$	176			
$A_g^{(5)}$	198				$B_{1g}^{(5)}$	185			B_{2g}
$A_g^{(6)}$	210				$B_{1g}^{(6)}$	188			
$A_g^{(7)}$	231	213/235	middle RuO_6 rot in xy	A_{1g}	$B_{1g}^{(7)}$	327	288/307	O3($z,-z$)	B_{2g}
$A_g^{(8)}$	234				$B_{1g}^{(8)}$	327			
$A_g^{(9)}$	286				$B_{1g}^{(9)}$	354	373/388	O3(xy)	B_{2g}
$A_g^{(10)}$	288				$B_{1g}^{(10)}$	356			
$A_g^{(11)}$	309				$B_{1g}^{(11)}$	464			B_{2g}
$A_g^{(12)}$	313				$B_{1g}^{(12)}$	464			
$A_g^{(13)}$	358	361/372	O3(z)	A_{1g}	$B_{1g}^{(13)}$	476			
$A_g^{(14)}$	364				$B_{1g}^{(14)}$	476			
$A_g^{(15)}$	512	533/	O3(xy)	A_{1g}	$B_{1g}^{(15)}$	482			
$A_g^{(16)}$	514				$B_{1g}^{(16)}$	482			
$A_g^{(17)}$	552	584/588	O2(z)	A_{1g}	$B_{1g}^{(17)}$	708			
$A_g^{(18)}$	562				$B_{1g}^{(18)}$	708			
$A_g^{(19)}$	678	745/	O1(z)	A_{1g}					
$A_g^{(20)}$	678								

for light polarization parallel to the *ab* plane. This is shown in more detail in the right panels of Fig. 11.

The ferromagnetic ordering at $T = 105$ K has a moderate, but clearly pronounced effect on phonon parameters and electron–phonon interaction. The temperature dependencies of the position (Fig. 12a), width (Fig. 12b), and q-parameter of the Fano shaped B_{1g} line, corresponding to O3 vibrations in the xy plane, change their slope near T_C. Although the relative changes of $\Gamma(T)|q(T)| \propto V(T)$ are relatively small, the well pronounced maximum near T_C (Fig. 12d) indicates that the electron–phonon coupling is affected by the magnetic ordering. The parameters of the second B_{1g} line, corresponding to O3 vibrations in z direction exhibit no detectable anomaly near T_C (Fig. 12e and f).

The magnetic ordering may affect phonon frequency through different mechanisms: exchange striction [22,15], dependence of the spin energy on ion displacements [22–24], variations of the density of itinerant carriers near T_M [14]. Although consistent with observation of anomaly in $V(T)$, the latter mechanism, proposed to explain the anomalous hardening near T_C of several Raman modes in ferromagnetic $SrRuO_3$, is irrespective to the bond lengths and band angles being modulated and seems to be of less importance in $Sr_4Ru_3O_{10}$. The observation of detectable anomaly near T_C

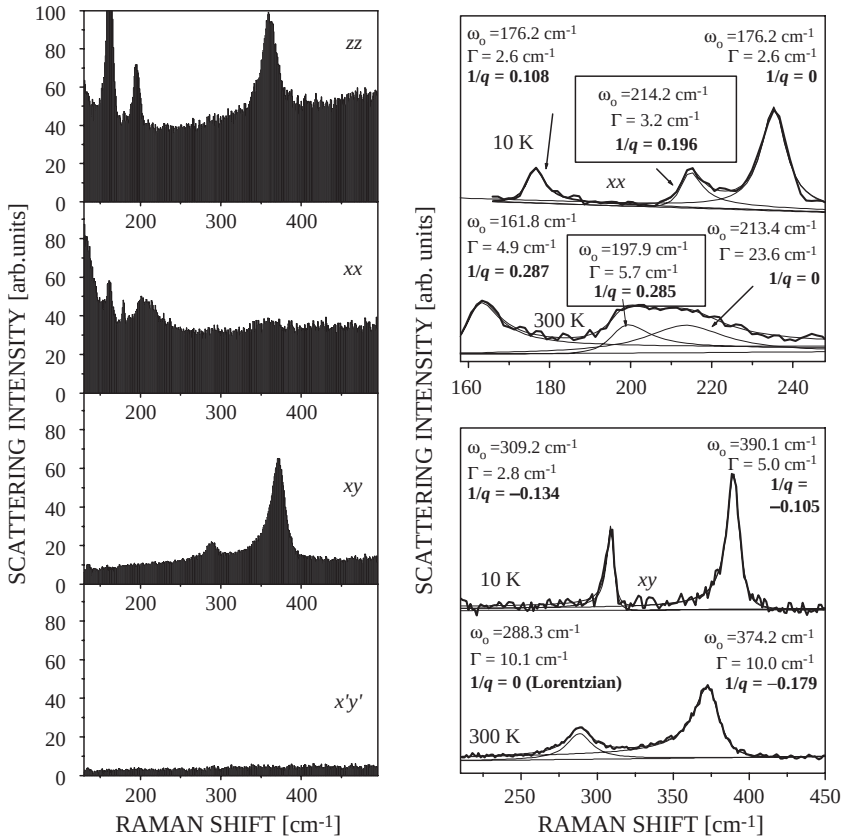

Fig. 11. Left panel: continuum scattering in the spectra of $Sr_4Ru_3O_{10}$ obtained with 633 nm excitation. Right panels: Fano fits $xx(A_g)$ and $xy(B_{1g})$ spectra of $Sr_4Ru_3O_{10}$ obtained with 515 nm excitation at 10 and 300 K. The fit parameters are also given.

only for modes, which modulate the Ru1-O3-Ru1 angle, rather favors direct interaction of these phonons with the magnetization [22,24].

5. Conclusions

We studied in detail the polarized Raman spectra of Sr_2RuO_4, $Sr_3Ru_2O_7$ and $Sr_4Ru_3O_{10}$ with particular attention to the two latter compounds as their phonon spectra have not been reported so far. All observed Raman lines are of either A_g or B_{1g} symmetry. They have been assigned to definite atomic vibrations by: (1) considering the Raman active modes in simplified tetragonal $P4/nbm$ and $P4/mbm$ structures, which contain only one double or triple RuO_6 layers per unit cell and account for the rotational distortions, (2) comparison to the predictions of lattice dynamical calculations for the real orthorhombic double layer Pbna and triple layer Pbam structures. Except for the discrete phonon lines, a continuum background, presumably of electronic origin, is present in the *zz*, *xx* and *xy*, but not in the *x′y′* and *zx* spectra. The interaction of *xx* and *xy* continuum with the modes involving atomic motions in the *ab* plane results in Fano shape of corresponding Raman lines. While no anomaly in phonon parameters of $Sr_3Ru_2O_7$ is seen between 10 and 300 K, where no magnetic transition

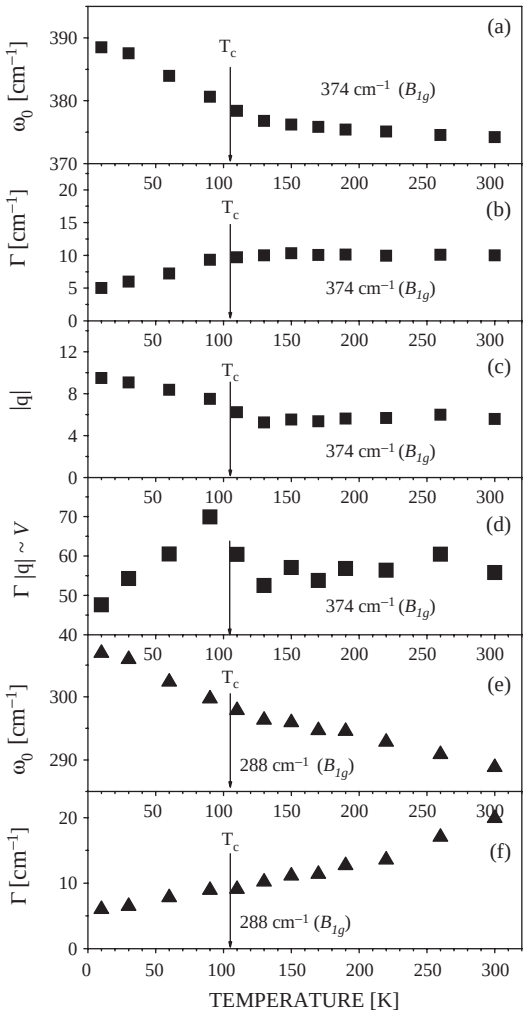

Fig. 12. Variations with T of (a): ω_0, (b): Γ, (c): $|q|$ and (d): $\Gamma q \propto V$ for the Fano shaped B_{1g} line at 374/389 cm^{-1}. No anomaly near T_C is observed, however, for the position (e) and the width (f) of the Lorentzian B_{1g} line at 288/308 cm^{-1}.

occurs, an anomaly is observed near ferromagnetic transition at 105 K in $Sr_4Ru_3O_{10}$.

Acknowledgements

This work is supported in part by the state of Texas through the Texas Center for Superconductivity and Advanced Materials, by NSF grant no. DMR-9804325, the T.L.L. Temple Foundation, the J. J. and R. Moores Endowment, and at LBNL by the Director, Office of Energy Research, Office of Basic Energy Sciences, Division of Materials Sciences of the US Department of Energy under contract no. DE-AC03-76SF00098. J.B. acknowledges financial support from the Swedish Superconductivity Consortium.

References

[1] Y. Maeno, T.M. Rice, M. Sigrist, Phys. Today 54 (1) (2001) 42.
[2] M. Braden, Y. Sidis, P. Bourges, P. Pfeuty, J. Kulda, Z. Mao, Y. Maeno, Phys. Rev. B 66 (2002) 064522.
[3] S.-I. Ikeda, Y. Maeno, S. Nakatsuji, M. Kosaka, Y. Uwatoko, Phys. Rev. 62 (2000) R6089.
[4] Q. Huang, J.W. Lynn, R.W. Erwin, J. Jarupatrakorn, R.J. Cava, Phys. Rev. B 58 (1998) 8515.
[5] M.K. Crawford, R.L. Harlow, W. Marshall, Z. Li, G. Cao, R.L. Lindstrom, Q. Huang, J.W. Lynn, Phys. Rev. B 65 (2002) 214412.
[6] G. Cao, L. Balicas, W.H. Song, Y.P. Sun, Y. Xin, V.A. Bondarenko, J.W. Brill, S. Parkin, X.N. Lin, Phys. Rev. B 68 (2003) 174409.
[7] G. Cao, K. Abbound, S. McCall, J.E. Crow, R.P. Guertin, Phys. Rev. B 62 (2000) 998.
[8] H. Shaked, J.D. Jorgensen, S. Short, O. Chmaissem, S.-I. Ikeda, Y. Maeno, Phys. Rev. B 62 (2000) 8725.
[9] C.S. Snow, S.L. Cooper, G. Gao, J.E. Crow, H. Fukazawa, S. Nakatsuji, Y. Maeno, Phys. Rev. Lett. 89 (2002) 226401.
[10] H.L. Liu, S. Yoon, S.L. Cooper, G. Cao, J.E. Crow, Phys. Rev. B 60 (1999) R6980.
[11] S. Sakita, S. Nimori, Z.Q. Mao, Y. Maeno, N. Ogita, M. Udagawa, Phys. Rev. B 63 (2001) 134520.
[12] H. Rho, S.L. Cooper, S. Nakatsuji, H. Fukazawa, Y. Maeno, Phys. Rev. B 68 (2003) 100404(R).
[13] V.N. Popov, J. Phys.: Condens. Matter 7 (1995) 1625.
[14] M.N. Iliev, A.P. Litvinchuk, H.-G. Lee, C.L. Chen, M.L. Dezaneti, C.W. Chu, V.G. Ivanov, M.V. Abrashev, V.N. Popov, Phys. Rev. B 59 (1999) 364.
[15] M. Udagawa, T. Minami, N. Ogita, F. Nakamura, T. Fujita, J.G. Bednorz, F. Lichtenberg, Physica B 219 & 220 (1996) 222.
[16] A. Yamanaka, N. Asayama, M. Sasada, K. Inoue, M. Udagawa, S. Nishizaki, Y. Maeno, T. Fujita, Physica C 263 (1996) 516.
[17] M. Kakihana, S.-G. Eriksson, L. Börjesson, L.G. Johansson, C. Ström, M. Käll, Phys. Rev. B 47 (1993) 5359.
[18] Y.K. Atanassova, V.G. Hadjiev, P. Karen, A. Kjekshus, Phys. Rev. B 50 (1994) 586.

[19] J.J. Neumeier, M.F. Hundley, M.G. Smith, J.D. Thompson, C. Allgeier, H. Xie, W. Yelon, J.S. Kim, Phys. Rev. B 50 (1994) 17910.
[20] A.V. Puchkov, Z.-X. Shen, G. Cao, Phys. Rev. B 58 (1998) 6671.
[21] D.J. Singh, I.I. Mazin, Phys. Rev. B 63 (2001) 165101.
[22] W. Baltensperger, J.S. Helman, Helv. Phys. Acta 41 (1968) 668.
[23] M. Udagawa, K. Kohn, N. Koshizuka, T. Tsushima, K. Tsushima, Solid State Commun. 16 (1975) 779.
[24] X.K. Chen, J.C. Irwin, J.P. Franck, Phys. Rev. B 52 (1995) R13130.